ESIPT in the pyrrol pyridine molecule: mechanism, timescale and yield revealed using dynamics simulations

Anthony Ferté, Axel Houssin, Nina Albouy, Isabella Merritt, Morgane Vacher

Journal Name

ARTICLE TYPE

Cite this: DOI: 00.0000/xxxxxxxxxx

ESIPT in the Pyrrol Pyridine molecule: Mechanism, timescale and yield revealed using dynamics simulations†

Anthony Ferté[a], Axel Houssin[a], Nina Albouy[a,b], Isabella C. D. Merritt[a] and Morgane Vacher[a]*

Received Date
Accepted Date

DOI: 00.0000/xxxxxxxxxx

Excited State Intramolecular Proton Transfer in Pyrrol Pyridine is theoretically investigated using non-adiabatic dynamics simulations. The photochemical process is completely characterised: the reaction time, the total yield and the accessibility of the conical intersection are evaluated. Finally, new mechanistic interpretation are extracted: the proton transfer reaction in this molecule is shown to be driven by two complementary mechanisms.

Excited State Intramolecular Proton Transfer (ESIPT) is one of the most striking photochemical processes, thanks to its remarkable properties, its wide range of applications, and its central role in various biological mechanisms and in the photostability of natural molecular systems.[1–3] This process, first observed on salicylic acid,[4] occurs when an electronic excited state is associated with a different most stable tautomer from the one on the electronic ground state. Such molecules may thus undergo excitation-induced proton transfer. Usually, this transfer occurs along a pre-existing hydrogen bond that greatly favours the tautomerization. The ESIPT process is considered to be quite fast[5], typically on the sub-100 femtoseconds timescale. Molecular properties can however significantly modulate the ESIPT speed and efficiency.

One useful distinction is between "*ballistic*" and bi-stable ESIPT systems[2,6–10]. In the first case, the excited state potential energy surface (PES) displays only one stable well associated with the proton transfer tautomer. The excited molecule collapses quickly and entirely, in a ballistic-like fashion, toward the photoproduct. The significant reorganization of the molecule leads to a large Stokes shift, characteristics of ESIPT chromophores. In the second case, bi-stable ESIPT molecules are characterized by a double well PES on the excited state: one well corresponding to the reactant tautomer and a second to the product. The presence of an activation barrier can lead to notable reduction of the ESIPT rate and yield in comparison to the ballistic case. Partial tautomerisation can result in emission spectra displaying two bands: one slightly Stokes shifted corresponding to the molecules in the reactant well, and a second significantly Stokes shifted corresponding to the ESIPT product. Dual-emissive bi-stable ESIPT molecules have been notably suggested as promising candidates to develop color-tunable as well as white light emitting chromophores.[11–18] Understanding how the proton transfer occur in such system is thus a goal of major interest.

Experimentally, ESIPT yields and reaction times can be extracted from fluorescence intensity ratio and time-resolved spectroscopies,[5,6,19–25] while transient absorption measurements allow to observe the signature of vibrational modes involved in the proton transfer.[19,21,26,27]

Theoretical investigations have been performed on multiple types of ESIPT molecules employing various computational approaches.[2] Most of them relied on static calculations aimed at characterizing the different tautomers, key points of the PES (transition state, conical intersections, etc.) and minimal energy reaction paths. To this end, Time-Dependent Density Functional Theory (often with implicit solvent model), Green's function based ADC(2), Coupled Cluster based CC2, and Complete Active Space Self Consistent Field with and without second order perturbative correction (CASSCF/CASPT2) are the most commonly employed methods.[7,15,22,28–36] Notably, vibronic transition computations have been used to simulate optical properties of ESIPT tautomers[7,37,38] and assess ESIPT yields by adjusting the relative weight of the two emission bands in order to reproduce experimental spectra.[7] However, such a procedure only leads to an "apparent" ESIPT yield, since non-radiative quenching cannot be distinguished from population ratio effects.

Dynamics methods on the other hand allow the explicit simulation of the proton transfer reaction. Full quantum dynamics methods such as Multi-Configuration Time-Dependent Hartree (MCTDH)[39–44] and semi-classical approaches such as Ab Initio Multiple Spawning (AIMS)[45,46] and surface hopping (with decoherence correction)[47–53] have been applied to investigate ESIPT.

[a] *Nantes Université, CNRS, CEISAM, UMR 6230, F-44000 Nantes, France*
[b] *Département de Chimie, École Normale Supérieure, PSL University, 75005 Paris, France*
* *E-mail: morgane.vacher@univ-nantes.fr*

† Electronic Supplementary Information (ESI) available: Static results, Active orbitals, Time evolution along other relevant nuclear coordinates. See DOI: 00.0000/00000000.

The Nuclear Electronic Orbital (NEO) method, which allows the full quantum treatment of a restricted set of nuclei (usually hydrogen), is a promising alternative in that context.[54] Dynamics simulations have also been coupled with machine learning based analysis methods to extend the available physical insight.[55,56]

We present here a theoretical investigation of the ESIPT reaction in the 2-(1H-pyrrol-2-yl)pyridine molecule (PP; see figure 1) using extensive dynamic simulations, to assess the characteristics of the proton transfer in this system. PP falls in the category of the bi-stable ESIPT molecules, with two stable wells in the excited state.[35,37,49,57] This is confirmed by our own static calculations performed at the CASPT2(10e,8o)/ANO-RCC-VDZP level of theory (see ESI) predicting an activation barrier for the ESIPT of about 0.27 eV. This is in reasonable agreement with the previously mentioned theoretical literature, as well as experimental investigations indicating an activation barrier of about 0.13 eV in n-hexane.[58] CASPT2 also predicts that about 0.49 eV of potential energy should be "stored" in the system after vertical excitation. A large ESIPT yield is thus expected since this available energy is larger than the activation barrier, and the barrier in the direction of the reverse proton transfer is large (1.44 eV).

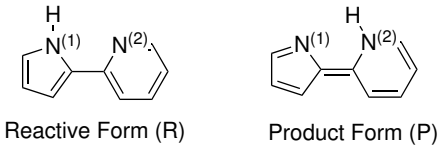

Fig. 1 Reactant and Product tautomer structures of the PP molecule.

The dynamical aspects of the ESIPT reaction in the PP molecule are investigated using the semi-classical surface hopping method[59,60]. In this approach, the quantum delocalisation of the nuclear wavepacket is recovered *via* the use of a swarm of classical trajectories, while the splitting of the wavepacket onto different electronic states is mimicked by allowing each individual trajectory to hop from one PES to another. Li *et. al.* previously used this approach to illustrate their static investigation of the ESIPT in PP by simulating few trajectories over a short period of time.[49] In the present work, a large set of 100 trajectories is used to allow the inference of mechanistic information and the simulation is performed over a period of 1 ps when the system seems to stabilize. The simulations are run using the Newton-X software[61] with a 0.5 fs time-step. The starting points (geometry and velocities) are generated from a Wigner sampling of the ground state nuclear wavepacket. Trajectories that display unphysical total energy variation along the dynamics (only 14 of them) are discarded according to the default procedure used in Newton- X albeit with tighter thresholds (0.4 eV for the total variation and 0.2 eV over a single time step). The electronic structure calculations are performed at the ADC(2) level using the Turbomole software.[62] This choice of electronic structure method is motivated by the fact that the proton transfer occurs adiabatically on the excited state within a geometrical space where ground and first excited states stay well separated.[35] Therefore, the theoretical description of the ESIPT process should not be impeded by the limitations of the method regarding the description of electronic degeneracy regions. Although ADC(2) is expected to yield reasonable PES shape in the vicinity of the twisted conical intersection accessible after the ESIPT,[63] the proportion of trajectories still in the excited state is assessed by counting the trajectories far from the electronic degeneracy (*i.e.* $\Delta E_{S_0/S_1} > 0.1$ eV).

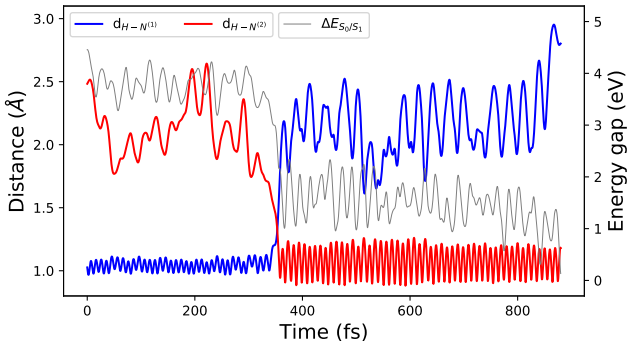

Fig. 2 Example of typical reactive trajectory observed in the simulations. (Blue) Distance between the proton and the donor nitrogen $N^{(1)}$. (Red) Distance between the proton and the acceptor nitrogen $N^{(2)}$. (Grey) Energy gap between electronic ground and excited states.

Figure 2 shows a typical case of a reactive trajectory observed in the simulations. Initially, the molecule remains within the reactant well as evidenced by the fast oscillations of the proton-donor distance (blue curve) with a frequency corresponding to the typical N–H bond stretching (*ca.* 3500 cm^{-1} *i.e.* a period of roughly 9.5 fs).[64] In this specific trajectory the proton transfer occurs 353.5 fs after excitation. This time corresponds to the instant at which the proton-acceptor distance (red curve) becomes smaller than the proton-donor one. One can notice that the proton transfer is accompanied by a reduction of the ground-excited state energy gap (grey curve) clearly illustrating the large Stokes shift characteristic of ESIPT chromophores. The molecule evolves then in the product tautomer well (it is now the proton-acceptor distance that displays the characteristic N–H bond stretching frequency). The conical intersection is finally reached after 880.5 fs at which point the molecule is considered to decay non-radiatively to the electronic ground-state. One can notice the increase of the proton-donor distance due to the twisted geometry of the conical intersection[35] (see ESI for an analysis of all the geometries near degeneracy encountered over the entire set of trajectories).

Over the ensemble of trajectories, an average ESIPT time of 274.45 fs is observed with a large standard deviation of 256.1 fs. The total populations of the two tautomers are evaluated at each time step and reported in Figure 3 (blue: reactant tautomer; red: product tautomer). The number of excited state trajectories, *i.e.* the trajectories that have not reached the conical intersection (and not been discarded due to energy non-conservation) is also reported (grey line). As expected, a fast decay of the reactant population can be observed starting about 50 fs after excitation. One can also notice a slower but clear decrease in the number of active trajectories illustrating that most of the trajectories that have undergone the proton transfer also tend to reach the conical intersection within the time of the simulation (54 out of 66 reactive trajectories). An important quenching of the product tautomer

fluorescence is thus to be expected, a fact in agreement with the small experimental intensity of the photoproduct signal.[57,58]

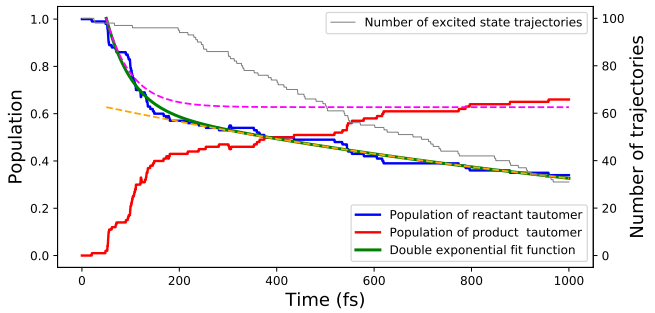

Fig. 3 Evolution of the PP tautomer populations upon electronic excitation: reactant (blue) and product (red). The reactant population curve was fitted using a sum of two exponential decay functions (green), each exponential function being also individually plotted (dashed pink and orange). The grey line represents the number of excited state trajectories.

The decaying reactant tautomer population is fitted using a bi-exponential function that returns 1 at $t = t_0$ (optimised at 50.4 fs), decays with two characteristic half-life times of $(\ln(2) \times a)$ and $(\ln(2) \times d)$ and reaches an asymptotic population of $|c|$:

$$f(t) = (1 - b - |c|) \exp\left(\frac{-(t - t_0)}{a}\right) + b \exp\left(\frac{-(t - t_0)}{d}\right) + |c|. \quad (1)$$

Our simulations show that the PP molecule displays a first fast initial proton transfer rate (pink dashed curve; exponential decay half-life of 36.0 fs). This is in qualitative agreement with the findings of Li *et al.*[49] who reported that 25 out of their 30 trajectories had experienced ESIPT after 300 fs. However, our simulations indicate that most of the molecules do not undergo this pathway. Instead, at later time, the system experiences a second slower ESIPT rate (orange dashed curve; exponential decay half-life of 1008.5 fs). The extremely low asymptotic reactant population extracted from our fitting procedure ($|c| = 1.04 \times 10^{-6}$) suggests an almost total proton transfer yield for the PP molecule. However, given the long exponential decay time associated with this second mechanism, one would need to extend the simulation time to obtain a more precise prediction of the asymptotic yield.

On top of the general trends discussed before, the tautomer populations (Figure 3) present regular step-like structures. This feature of the curves remains visible when restricting our analysis to fewer number of trajectories, thus indicating that these structures are not a statistical artifact. Such observation indicates that a pseudo-periodic evolution of the molecule favours the appearance of "batches" of nearly simultaneous proton transfers.

Figure 4 shows the time evolution of the distribution in distance between the proton and the acceptor nitrogen (r), over the whole set of excited state trajectories. Similar plots along other coordinates are reported in the ESI. There are clearly two intervals of r in which the molecule is most likely to be found during the dynamics: 2.5-1.75 Å corresponding to the reactant tautomer well and 1.25-0.8 Å corresponding to the product one. Unsurprisingly, all the trajectories are initially found within the reactant tautomer interval. The later appearance of trajectories within the product interval is here the signature of the proton transfer occurring.

More precisely, the initial distribution of r is centered around the optimal proton-acceptor distance in the electronic ground state which was estimated at 2.392 Å from the CASPT2 calculations. This optimal distance is reduced to about 2.108 Å in the excited state, thus explaining the significant initial drop in the average value of r. Following this, one observes a coherent oscillation of the molecule in the reactant well. From the distribution of the proton transfer events (white dots), one can infer that for a proton transfer to occur, r necessarily needs to be on the very low edge of the reactant tautomer interval. However, the molecular distribution within that region is quite sparse. Therefore, the probability of proton transfer is highly dependent on the previously mentioned ensemble motion that globally steers the system towards the reactive region. One can observe a clear concentration of white dots when the distribution of r extends towards lower values. As a result, the apparent pseudo-periodicity of roughly 200 fs that can be observed in the distribution of r matches the roughly 200 fs time delay between the successive step-like structures observed in Figure 3. Finally, there is a connection between this global motion and the two apparent reaction rates observed previously. Indeed, the transition between the two decay regimes (dashed curves in Figure 3) occurs slightly before the 200 fs mark, roughly corresponding to the end of the first "oscillation" along r. Thus, the initial fast rate corresponds to proton transfer reactions induced by the initial decrease in the global proton-acceptor distance due to the geometrical relaxation of the molecule in the excited state. This ballistic-like mechanism is similar to what is observed in the case of a barrier-less ESIPT where the molecule is naturally guided toward the tautomer by the gradient of the PES. However, in the present case, this balistic-like ESIPT is not total and accounts for about 40% of the chromophores. On the other hand, the slower ESIPT rate observed at later time can be connected to the lingering coherent oscillatory motion in the reactant well of the excited state.

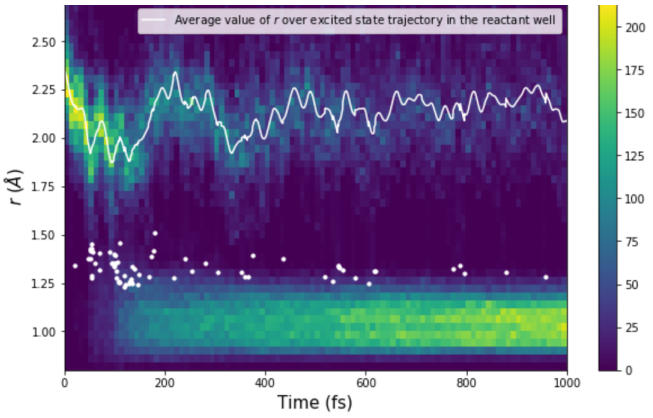

Fig. 4 (Top) Time evolution of the total distribution of r (distance between the proton and the acceptor nitrogen) over all trajectories. The white line represents the average value of r only taking into account excited state trajectories in the reactant tautomer well. White dots depict the value of r at each proton transfer time.

By performing dynamic calculations on the excited PP molecule, we successfully simulated how the ESIPT process occurs in this system. As expected from the small activation barrier

in regard to the potential energy stored in the excited molecule at the Franck-Condon geometry, a highly efficient reaction is observed. Indeed, an ESIPT yield of 66% was obtained after 1 ps. Although underestimation of the activation barrier with ADC(2) (see ESI) may yield to an overestimation of the yield, a large proton transfer yield is nonetheless expected. The simulations also revealed the relative ease with which the product can reach the twisted conical intersection synonymous with photoproduct fluorescence quenching. Indeed, more than 80% of the reactive trajectories reached the twisted conical intersection within the simulation time. Importantly, the ESIPT in PP is driven by two complementary mechanisms. First a ballistic-like process is induced by the initial geometrical relaxation of the system on the excited state, leading to an initial fast ESIPT rate and proton transfer events in about 40% of all molecules. Then, a second mechanism, driven by the lingering coherent oscillatory nuclear motion of the molecule in the reactant well of the excited state, dominates at longer time and leads to periodic-like increases in the ESIPT probability and an overall slower reaction rate.

Acknowledgments

The authors are grateful to Denis Jacquemin for his assistance with the use of Turbomole. M.V. thanks the *Région des Pays de la Loire* who provided post-doctoral funding for A.F. and a Master scholarship for A.H. through the *Étoiles montantes* and PULSAR programs. I.C.D.M. acknowledges thesis funding from Nantes Université. This work was performed using HPC resources from GENCI-IDRIS (Grant 2022-101353) and CCIPL (Le centre de calcul intensif des Pays de la Loire).

Conflicts of interest

There are no conflicts of any sort to declare.

References

1 H. C. Joshi and L. Antonov, Molecules, 2021, **26**, 1475.
2 J. Jankowska and A. L. Sobolewski, Molecules, 2021, **26**, 5140.
3 T. Stoerkler, T. Pariat, A. D. Laurent, D. Jacquemin, G. Ulrich and J. Massue, Molecules, 2022, **27**, 2443.
4 A. Weller, Sci. Nat., 1955, **42**, 175–176.
5 K. K. Smith and K. J. Kaufmann, J. Phys. Chem., 1981, **85**, 2895–2897.
6 P. Wnuk, G. Burdziński, M. Sliwa, M. Kijak, A. Grabowska, J. Sepioł and J. Kubicki, Phys. Chem. Chem. Phys., 2014, **16**, 2542–2552.
7 Y. Houari, A. Charaf-Eddin, A. D. Laurent, J. Massue, R. Ziessel, G. Ulrich and D. Jacquemin, Phys. Chem. Chem. Phys., 2014, **16**, 1319–1321.
8 G. A. Parada, T. F. Markle, S. D. Glover, L. Hammarström, S. Ott and B. Zietz, Chem. Eur. J., 2015, **21**, 6362–6366.
9 Z.-Y. Liu, J.-W. Hu, T.-H. Huang, K.-Y. Chen and P.-T. Chou, Phys. Chem. Chem. Phys., 2020, **22**, 22271–22278.
10 Y.-H. Liu, S.-B. Yu, Y.-J. Peng, C.-W. Wang, C. Zhu and S.-H. Lin, RSC Adv., 2021, **11**, 37299–37306.
11 K.-C. Tang, M.-J. Chang, T.-Y. Lin, H.-A. Pan, T.-C. Fang, K.-Y. Chen, W.-Y. Hung, Y.-H. Hsu and P.-T. Chou, J. Am. Chem. Soc., 2011, **133**, 17738–17745.
12 D. Yao, S. Zhao, J. Guo, Z. Zhang, H. Zhang, Y. Liu and Y. Wang, J. Mater. Chem., 2011, **21**, 3568–3570.
13 K.-I. Sakai, T. Ishikawa and T. Akutagawa, J. Mater. Chem. C, 2013, **1**, 7866.
14 K. Benelhadj, W. Muzuzu, J. Massue, P. Retailleau, A. Charaf-Eddin, A. D. Laurent, D. Jacquemin, G. Ulrich and R. Ziessel, Chem. Eur. J., 2014, **20**, 12843.
15 C. Azarias, S. Budzák, A. D. Laurent, G. Ulrich and D. Jacquemin, Chem. Sci., 2016, **7**, 3763–3774.
16 Z. Zhang, Y.-A. Chen, W.-Y. Hung, W.-F. Tang, Y.-H. Hsu, C.-L. Chen, F.-Y. Meng and P. T. Chou, Chem. Mater., 2016, **28**, 8815–8824.
17 I. E. Serdiuk, J. Phys. Chem. C, 2018, **122**, 18615–18620.
18 E. S. Moraes, L. G. T. A. Duarte, J. C. Germino and T. D. Z. Atvars, J. Phys. Chem. C, 2020, **124**, 22406–22415.
19 S. Lochbrunner, A. Szeghalmi, K. Stock and M. Schmitt, J. Chem. Phys., 2005, **122**, 244315.
20 J. Lee, C. H. Kim and T. Joo, J. Phys. Chem. A, 2013, **117**, 1400–1405.
21 J. Kim, W. Heo and T. Joo, J. Phys. Chem. B, 2015, **119**, 2620–2627.
22 M. G. Vivas, J. C. Germino, C. A. Barboza, D. d. A. Simoni, P. A. M. Vazquez, L. De Boni, T. D. Z. Atvars and C. R. Mendonça, J. Phys. Chem. C, 2017, **121**, 1283–1290.
23 S. Ameer-Beg, S. M. Ormson, R. G. Brown, P. Matousek, M. Towrie, E. T. J. Nibbering, P. Foggi and F. V. R. Neuwahl, J. Phys. Chem. A, 2001, **105**, 3709.
24 A. N. Bader, F. Ariese and C. Gooijer, J. Phys. Chem. A, 2002, **106**, 2844–2849.
25 P. Todorov, D. Georgieva, P. Peneva, R. Rusew, B. Shivachev and A. Georgiev, New J. Chem., 2020, **44**, 15081–15099.
26 Y. Yoneda, H. Sotome, R. Mathew, Y. A. Lakshmanna and H. Miyasaka, J. Phys. Chem. A, 2020, **124**, 265–271.
27 J. W. Kim, C. H. Kim, C. Burger, M. Park, M. F. Kling, D. E. Kim and T. Joo, J. Phys. Chem. Lett., 2020, **11**, 755–761.
28 M. N. Khimich, V. L. Ivanov, M. Y. Melnikov, I. V. Shelaev, F. E. Gostev, V. A. Nadtochenko and B. M. Uzhinov, Photochem. Photobiol. Sci., 2017, **16**, 1139.
29 P. M. Vérité, S. Hédé and D. Jacquemin, Phys. Chem. Chem. Phys., 2019, **21**, 17400–17409.
30 N. Zhang, D. Liu, W. Chen and J. Yan, Comput. Theor. Chem., 2020, **1185**, 112898.
31 M. Ni, S. Su and H. Fang, J. Mol. Model., 2020, **26**, 108.
32 A. Chrayteh, C. P. Ewels and D. Jacquemin, Phys. Chem. Chem. Phys., 2020, **22**, 854–863.
33 A. Chrayteh, C. P. Ewels and D. Jacquemin, Phys. Chem. Chem. Phys., 2020, **22**, 25066–25074.
34 C. A. Barboza, P. Gawrys, M. Banasiewicz, K. Suwinska and A. L. Sobolewski, Phys. Chem. Chem. Phys., 2020, **22**, 6698–6705.
35 M. F. Rode and A. L. Sobolewski, Chem. Phys., 2008, **347**, 413–421.
36 D. Wu, W.-W. Guo, X.-Y. Liu and G. Cui, Chem. Phys. Chem., 2016, **17**, 2340.
37 P. O. Hubin, A. D. Laurent, D. P. Vercauteren and D. Jacquemin, Phys. Chem. Chem. Phys., 2014, **16**, 25288–25295.
38 P. M. Vérité, C. A. Guido and D. Jacquemin, Phys. Chem. Chem. Phys., 2019, **21**, 2307–2317.
39 J. M. Ortiz-Sánchez, R. Gelabert, M. Moreno and J. M. Lluch, J. Chem. Phys., 2007, **127**, 084318.
40 A. Perveaux, M. Lorphelin, B. Lasorne and D. Lauvergnat, Phys. Chem. Chem. Phys., 2017, **19**, 6579–6593.
41 Y. Cao, J. Eng and T. J. Penfold, J. Phys. Chem. A, 2019, **123**, 2640–2649.
42 N. Anand, K. Welke, S. Irle and S. R. Vennapusa, J Chem. Phys., 2019, **151**, 214304.
43 N. Anand, S. V. K. Isukapalli and S. R. Vennapusa, J. Comput. Chem., 2020, **11**, 1068–1080.
44 N. Anand, P. Nag, R. K. Kanaparthi and S. R. Vennapusa, Phys. Chem. Chem. Phys., 2020, **22**, 8745–8756.
45 S. Pijeau, D. Foster and E. G. Hohenstein, J. Phys. Chem. A, 2017, **121**, 4595.
46 S. Pijeau, D. Foster and E. G. Hohenstein, J. Phys. Chem. A, 2018, **122**, 5555.
47 L. Spörkel, G. Cui and W. Thiel, J. Phys. Chem. A, 2013, **117**, 4574–4583.
48 J. Jankowska, M. Barbatti, J. Sadlej and A. L. Sobolewski, Phys. Chem. Chem. Phys., 2017, **7**, 5318–5325.
49 C. Li, D. Li, Y. Shi and Y. Liu, Org. Electron., 2018, **54**, 177–183.
50 D. Tuna, L. Spörkel, M. Barbatti and W. Thiel, Chem. Phys., 2018, **515**, 521–534.
51 S.-H. Xia, M. Che, Y. Liu, Y. Zhang and G. Cui, Phys. Chem. Chem. Phys., 2019, **19**, 10086–10094.
52 Y. Li, F. Siddique, A. J. A. Aquino and H. Lischka, J. Phys. Chem. A, 2021, **125**, 5765–5778.
53 P. Nag and S. R. Vennapusa, J. Photochem. Photobiol. A, 2022, **427**, 113767.
54 L. Zhao, A. Wildman, F. Pavošević, J. C. Tully, S. Hammes-Schiffer and X. Li, J. Phys. Chem. Lett., 2021, **12**, 3497–3502.
55 F. Häse, I. Fdez. Galván, A. Aspuru-Guzik, R. Lindh and M. Vacher, Chem. Sci., 2019, **10**, 2298–2307.
56 J. J. Goings and S. Hammes-Schiffer, ACS Cent. Sci., 2020, **6**, 1594–1601.
57 M. Kijak, A. Zielińska, C. Chamchoumis, J. Herbich, R. P. Thummel and J. Waluk, Chem. Phys. Lett., 2004, **400**, 279–285.
58 M. Kijak, Y. Nosenko, A. Singh, R. P. Thummel and J. Waluk, J. Am. Chem. Soc., 2007, **129**, 2738–2739.
59 J. C. Tully, J. Chem. Phys., 1990, **93**, 1061–1071.
60 S. Hammes-Schiffer and J. C. Tully, J. Chem. Phys., 1994, **101**, 4657–4667.
61 M. Barbatti, M. Ruckenbauer, F. Plasser, J. Pittner, G. Granucci, M. Persico and H. Lischka, Wiley Interdiscip. Rev. Comput. Mol. Sci., 2014, **4**, 26–33.
62 S. G. Balasubramani, G. P. Chen, S. Coriani, M. Diedenhofen, M. S. Frank, Y. J. Franzke, F. Furche, R. Grotjahn, M. E. Harding, C. Hättig, A. Hellweg, B. Helmich-Paris, C. Holzer, U. Huniar, M. Kaupp, A. Marefat Khah, S. Karbalaei Khani, T. Müller, F. Mack, B. D. Nguyen, S. M. Parker, E. Perlt, D. Rappoport, K. Reiter, S. Roy, M. Rückert, G. Schmitz, M. Sierka, E. Tapavicza, D. P. Tew, C. van Wüllen, V. K. Voora, F. Weigend, A. Wodyński and J. M. Yu, J. Chem. Phys., 2020, **152**, 184107.
63 A. Dreuw and M. Wormit, Wiley Interdiscip. Rev. Comput. Mol. Sci., 2015, **5**, 82–85.
64 N. Fuson, M.-L. Josien, R. L. Powell and E. Utterback, J. Chem. Phys., 1952, **20**, 145–152.